Design, near-field characterization, and modeling of 45° surface-plasmon Bragg mirrors

M. U. González,* J.-C. Weeber, A.-L. Baudrion, and A. Dereux

Laboratoire de Physique de l'Université de Bourgogne, UMR CNRS 5027, 9 avenue A. Savary, BP 47870, F-21078 Dijon, France

A. L. Stepanov and J. R. Krenn

Institute for Experimental Physics, Universität Karl Franzens, Universitätsplatz 5, A-8010 Graz, Austria

E. Devaux and T. W. Ebbesen

Laboratoire de Nanostructures, ISIS, Université Louis Pasteur, 8 allée Monge, BP 70028, F-67083 Strasbourg, France

The development of surface plasmon polariton (SPP) optical elements is mandatory in order to achieve surface plasmon based photonics. A current approach to reach this goal is to take advantage of the interaction of SPP with defects and design elements obtained by the micro- or nano-structuration of the metal film. In this work, we have performed a detailed study of the performance and behavior of SPP-Bragg mirrors, designed for 45° incidence, based on this approach. Mirrors consisting of gratings of both metal ridges on the metal surface and grooves engraved in the metal, fabricated by means of electron beam lithography and focused ion beam, have been considered. The performance of the mirrors has been characterized via near-field optical microscopy. An original procedure to obtain quantitative values of the mirrors' reflectivity and transmission coefficient from the near-field images is exposed. The mirrors composed of metal ridges are shown to act very efficiently, and a rather low number of elements (15 for the specific geometry studied) is able to deflect almost 100% of the incoming power. Conversely, the arrays of grooves produce a much lower reflectivity, which we attribute mostly to radiative scattering in the forward direction induced by the grooves. Besides, the considered systems have also been simulated by using the differential method. The results obtained from the numerical calculations present an excellent agreement with the experimental data, proving the reliability of this method to predict the behavior of this kind of systems while interacting with SPP. Based on the numerical modeling of the SPP-Bragg mirrors, the evolution of the mirrors' behavior with the ridges height is analyzed.

I. INTRODUCTION

In the last years, surface plasmon polaritons (SPP) have attracted an increasing attention as useful tools to achieve highly integrated optics.[1] The current tendency towards the down-sizing of photonic devices requires the control of light propagation beyond the diffraction limit, and the properties of SPP make them promising candidates as signal carriers. Basically, a surface plasmon polariton is an electromagnetic wave bound to the interface between two media featuring the real part of their dielectric functions of opposite signs, in general a metal and a dielectric.[2] SPP can propagate along the interface to which they are bound, their propagation length being of the order of tens of micrometers in the visible range and even higher (several hundreds of micrometers) in the infrared. The associated electromagnetic field is strongly enhanced at the interface and its amplitude decays exponentially into both neighboring media. This vertical confinement makes SPP very interesting for optical devices in coplanar geometry on the one hand, and also very sensitive to the surface features on the other hand. This last property provides a mechanism to control the propagation of surface plasmon polaritons: The interaction with surface defects,[3] process through which the SPP are reflected, transmitted and scattered both in SPP and in radiative light.

The control of the two-dimensional propagation of surface plasmons is indeed of fundamental importance to obtain SPP-based photonic devices, and the develop-ment of optical elements allowing this propagation control constitutes, therefore, a crucial step. So far, the interaction of SPP with surface defects has been studied both theoretically[4–6] and experimentally,[3,7,8] and it has been demonstrated that by means of the controlled micro-or nano-structuration of the metal surface several SPP optical elements can be obtained, e.g., SPP-waveguides,[9,10] mirrors,[11–13] lenses,[14] beamsplitters,[13] SPP-photonic bandgap crystals,[15,16] and light-SPP couplers.[17,18]

Although the feasibility of these optical elements is already shown, the progress of SPP-based photonics demands their optimization. This requires a systematic character-ization of the optical elements as well as a deeper under-standing of the interaction of the SPP with the surface de-fects. For example, SPP mirrors, and in particular SPP-Bragg mirrors, are by far the most analyzed system and, therefore, several configurations, such as gratings of metal ridges or grooves,[19] height[20] or width[21] modulations in long-range SPP-waveguides, gratings of slits,[12] or chains of dielectric particles[13] have been demonstrated to act as efficient mirrors. However, most of these studies, either experimental or theo-retical, are centered on the case of normal incidence on the SPP mirrors, thereby being limited to the one-dimensional situation.[12,19–21] Very few works take into account the highly necessary configuration of SPP deflection, that is, of chang-ing the direction of propagation along the metal flat surface.[13,22] Moreover, the validity of the theoretical and nu-merical analysis of the considered SPP optical elements has

still to be checked against the experimental data in order to assess their usefulness as modeling and predicting tools to optimize the elements design.

In this work, we have carried out the study of SPP mirrors, specifically SPP-Bragg mirrors, designed to reflect a surface plasmon polariton traveling on a gold thin film at 90°. Mirrors composed of two kind of defects have been considered: Gratings of gold protuberances (that we will denote ridges or lines in the following) and gratings of indentations (named slits or grooves). The response of the mirrors has been characterized in the near-field by means of photon scanning tunneling microscopy (PSTM),[23] a near-field microscopy mode very well suited for the imaging of SPP since it collects surface-bounded evanescent fields.[24] In addition, the study of the performance of the SPP mirrors in the near field also provides an insight of the local details of the interaction of the SPP and the mirrors. A procedure has been established in order to determine the mirrors' reflectivity and transmission coefficient from the near-field measurements, allowing one to obtain the reflectivity of the mirrors as a function of several structural parameters, such as the number of elements composing the mirrors or the kind of defects considered. Numerical calculations of the considered experimental configuration, based on the differential method[25,26] implemented with the S-matrix propagation algorithm and the fast Fourier factorization method,[27–32] have also been performed. The results obtained from the numerical simulations show a good agreement with the experimental data, demonstrating the validity of these calculations to improve the understanding of the interaction of SPP with surface defects and to further optimize the design of SPP-Bragg mirrors as well as other kinds of optical elements.

The paper is organized as follows: After the description of the fabrication procedure of the SPP mirrors and of the near-field microscope used to characterize them (Sec. II), we show in Sec. III A the experimental results on SPP-Bragg mirrors consisting of gratings of both Au ridges and slits. Section III B presents the numerical simulations of the considered structures based on the differential method, and the obtained results are compared to the experiments. Once the validity of the simulations is established, Sec. IV draws several conclusions on the mirrors' behavior by a combined exploitation of numerical and experimental data.

II. EXPERIMENTAL

Resulting from the interaction with a defect at the interface between a dielectric and a thin metal film, a surface plasmon polariton propagating along this interface is either reflected, transmitted or scattered both into SPP and radiative light. The SPP mirrors considered in this work exploit this interaction. In order to reinforce the effect of the interaction, not isolated defects but gratings of defects are used, so that we are dealing with SPP-Bragg mirrors. In a Bragg mirror, the period of the grating is designed in such a way that, for a given incident wavelength, the grating collective scattering generates a gap in the SPP dispersion relation. At this wavelength, the propagation of a SPP across the grating is forbidden and, therefore, a high SPP reflection occurs. Figures 1(a)
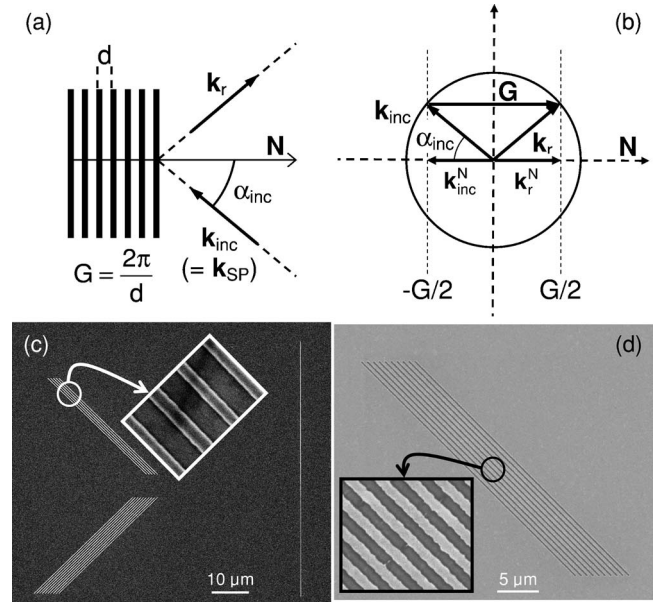

FIG. 1. Schematic diagram of a SPP-Bragg mirror in direct space (a) and in reciprocal space (b). (c) Scanning electron microscopy (SEM) image of two SPP-Bragg mirrors consisting of gratings of 5 (upper mirror) and 10 (bottom mirror) gold ridges. (d) SEM image of a SPP-Bragg mirror composed of a grating of 10 slits engraved in the gold film. All mirrors shown in (c) and (d) are designed for 45° incidence and SPP wavelength corresponding to a wavelength in vacuum equal to 800 nm, so the grating nominal period is 557 nm.

and 1(b) show schematic diagrams of a SPP-Bragg mirror in direct and reciprocal space, respectively. From Fig. 1(b) it can be seen that, in order to achieve Bragg reflection, the relation between the wave-vector of the incident SPP, $\mathbf{k}_{inc} \equiv \mathbf{k}_{SP}$ and the grating reciprocal vector, $\mathbf{G}$, should verify $\mathbf{k}_{inc} + \mathbf{G} = \mathbf{k}_r$. Thus, for Bragg mirrors designed for a given SPP wavelength, λ_{SP}, and angle of incidence, α_{inc}, the grating period, d, is given by:

$$d = \frac{\lambda_{SP}}{2 \cos \alpha_{inc}}. \tag{1}$$

The SPP-Bragg mirrors considered in this work have been designed for an angle of incidence of 45° and they consist of gratings of either gold ridges on gold thin films or slits engraved in the metal film. In the first case, the mirrors have been fabricated as follows: Initially, the gold ridges are obtained on an ITO-doped glass substrate by means of electron beam lithography (the nominal lines height is 70 nm), and a gold film, nominally 50 nm thick, is then evaporated on the whole substrate in order to obtain the extended metal film. For the obtention of mirrors comprised of gratings of slits, the glass is formerly coated by the gold layer, also nominally 50 nm thick, and the slits are then milled in the film with a focused ion beam. The slits go across the whole gold film. The typical width of both ridges and slits has been comprised in between 150 and 200 nm. Figures 1(c) and 1(d) show several of the fabricated SPP mirrors.

The characterization of the SPP interaction with the mirrors has been carried out by using a PSTM. The SPP in the gold film is excited by total internal reflection through the glass substrate (in the Kretschmann-Raether configuration) with a focused beam coming from a tunable Ti:sapphire laser. A multi-mode tapered optical fiber, coated with a thin metallic layer, is scanned at close vicinity of the sample surface, causing the frustration of the SPP evanescent field and, therefore, providing the mapping of the SPP electric field intensity on the sample surface. The use of metal coated tips has two main purposes: First, to shield the tip against radiative light that would add to the near-field optical signal; second, to supply, when a bias voltage is applied, an electronic tunnel current between the tip and the metal surface, which provides an absolute measurement of the tip-sample distance since this tunnel current occurs for the tip at quasi-contact with the surface. The images are taken by keeping the fiber tip at a constant distance, about 150 nm, from the sample surface. The tunability wavelength range of the Ti:sapphire laser being 740–830 nm, the Bragg mirrors have been designed for reflection of SPP excited with incoming light having a wavelength in vacuum of $\lambda_0 = 800$ nm, which implies that $\lambda_{SP} = 786$ nm and then the grating period (for 45° incidence) has to be $d = 557$ nm.

III. RESULTS

When a surface plasmon polariton travels along a metal-dielectric interface, the interaction with a surface defect gives rise to SPP reflection (which allows us to use arrays of controlled defects as SPP-Bragg mirrors) but also to radiative light scattered into the dielectric. We have taken advantage of this process in order to perform, in the far-field zone, a fast check of the ability of the fabricated SPP mirrors to change the propagation direction of an incident SPP. Figure 2(a) shows the scanning electron microscopy (SEM) image of the sample designed for this fast check. The SPP-Bragg mirror, designed for deflecting an incoming SPP with wavelength corresponding to $\lambda_0 = 800$ nm arriving at 45°, consists of an array of ten gold ridges, 75 nm high and 190 nm wide, and periodicity $d = 557$ nm. The mirror is surrounded by three single gold lines that will scatter part of a surface plasmon polariton traveling through them into radiative light. Figure 2(b) shows an image, recorded with an infrared CCD camera, of the scattered light when a SPP is launched towards the mirror. The white ellipse in Fig. 2(a) signals the place where the focused beam that excites the SPP is located, and the arrow indicates the propagation direction. In Fig. 2(b) we can observe: (1) A strong scattering spot in the right gold line, pointing out the crossing of the incident SPP; (2) a scattering area on the mirror, which marks the region of the mirror where the SPP hits; (3) a weaker scattering spot at the bottom gold line, revealing that a part of the SPP has been deflected at 90° from the incoming direction. No scattering spot can be detected in the left gold line (4), showing that a very small portion of the incident SPP is transmitted through the mirror.

The weaker intensity of the scattering spot associated to the reflected beam does not necessarily imply that the reflec-
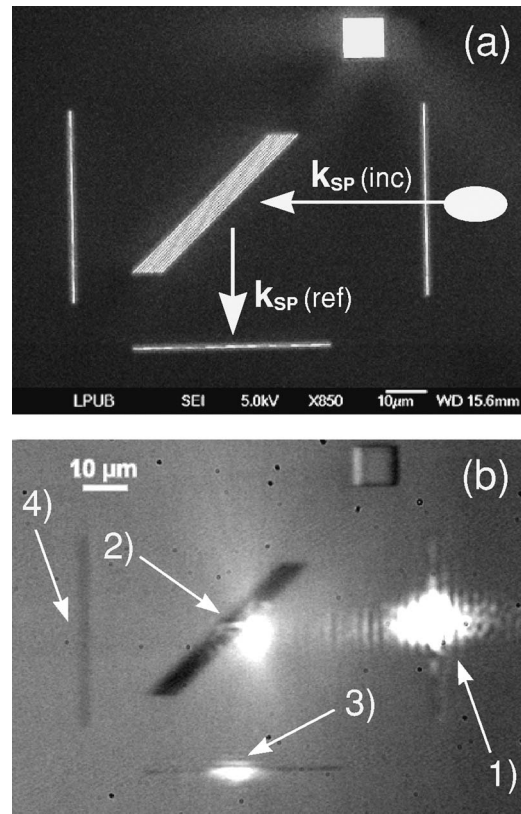

FIG. 2. (a) SEM image of a surface plasmon (SPP) Bragg mirror formed by 10 Au ridges (75 nm high and 190 nm wide), surrounded by Au lines (75 nm high and 200 nm wide) able to scatter into radiative light the SPP traveling through them. (b) Far-field image of a SPP being reflected by the mirror. The scattering spots are labeled as (1), (2), (3), and (4).

tivity of the mirror is low. The intrinsic damping of the SPP traveling along the gold film also plays a role. Indeed, the propagation length, L_{SP}, of a SPP traveling on a 50 nm thick gold film, defined as the distance for which the SPP field intensity decays to $1/e$ of his value,[2] is $L_{SP} \approx 25$ μm, calculated using the dielectric constant of gold from Ref. 33. Moreover, the gold lines included to detect the transmitted and reflected beams are placed at the same distance from the mirror, and therefore the image allows us to conclude unambiguously that the amount of SPP reflected by the mirror is much higher than the transmitted one. This far-field observation allows us to obtain a fast check of the capability of the considered gratings to act as SPP mirrors, but it offers neither a quantitative characterization of the mirrors' performance, nor a local detail of the interaction of the SPP with the mirror. In order to get this information, the near-field characterization of the mirrors has been carried out.

A. Near-field characterization of SPP-Bragg mirrors

Figure 3(a) shows a typical PSTM image of a SPP propagating on a gold thin film and interacting with a SPP-Bragg mirror. In this case, the mirror is equivalent to the one shown for the far-field check in Fig. 2: 10 gold ridges, 75 nm high and 190 nm wide, and a periodicity $d = 557$ nm again, as cor-
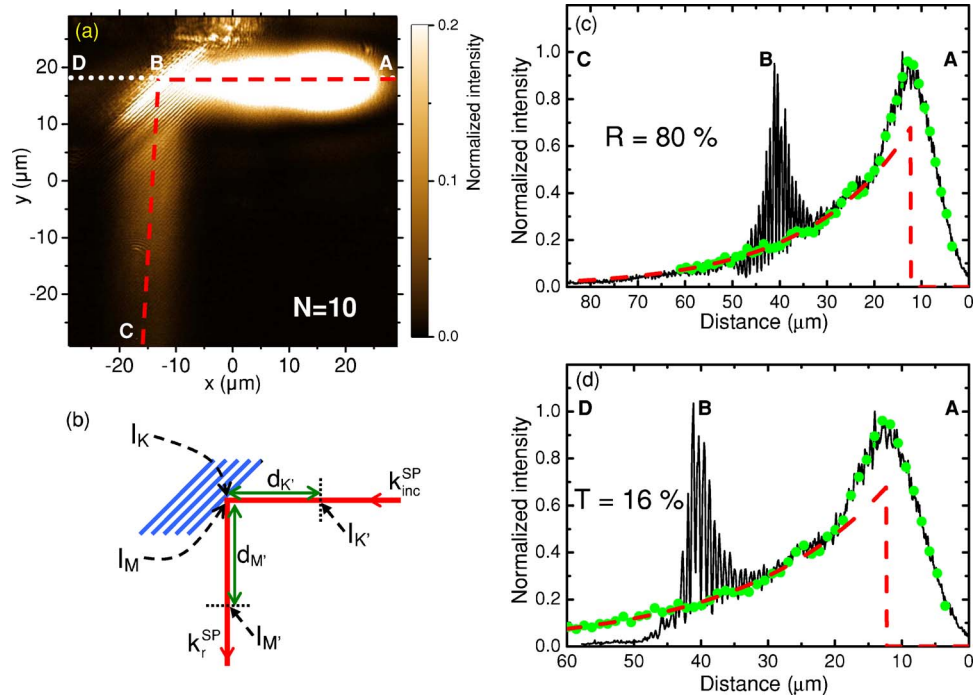
FIG. 3. (Color online) (a) Typical PSTM image of a surface plasmon (SPP) propagating from right to left along a gold thin film and interacting with a SPP Bragg mirror. The SPP-mirror comprises ten gold ridges, with a periodicity $d=557$ nm (designed for a SPP corresponding to $\lambda_0=800$ nm arriving at 45°). (b) Schematic diagram of the parameters involved in the SPP-mirrors' reflectivity calculation. (c) Solid black line: Intensity profile taken through the incident (A-B) and reflected (B-C) SPP beams [red dashed line drawn in (a)]. From this profile, the mirror reflectivity is calculated: $R=80\% \pm 14\%$ in this case. Dashed red line: Calculated intensity profile evolution for the incident SPP beam considering only the intrinsic damping. Dotted green line: Experimental intensity profile corresponding to a SPP launched close to the mirror, but not interacting with it. (d) Solid black line: Intensity profile taken through the incident (A-B) and transmitted (B-D) SPP beams [white dotted line in (a)]. From it, the obtained mirror transmission coefficient is $T=16\% \pm 3\%$. Dashed red line: As in (c). Dotted green line: As in (c).

responds to a mirror designed for SPP of $\lambda_0=800$ nm incoming at 45° incidence. An important difference between the samples fabricated for near-field characterization and those intended for far-field observation is that, in the former ones, the single gold lines surrounding the mirror are not included. In this way, we avoid the scattered radiative contribution provided by these single lines, some part of which could be captured by the probe tip thereby resulting in an over-estimation of the mirror reflectivity and transmission coefficient. As can be seen from the image, the SPP has been launched at approximately 29 μm from the mirror position, making an angle of 45° with the mirror normal. After interaction with the mirror, the SPP is deflected by 90°, as demonstrates the beam traveling towards the bottom of the image, and just a very small fraction of SPP has been transmitted through the mirror. The mirror position is clearly identified from the image, since it corresponds to the turning of the SPP.

From PSTM images of the SPP Bragg mirrors, such as that shown in Fig. 3(a), the mirrors' reflectivity and transmissivity can be quantified. Here it should be noticed that, since SPP propagate in a lossy medium, the reflectivity and transmission coefficient have only sense as local properties of the mirrors. Therefore, we understand the SPP mirrors reflectivity (and analogously the transmissivity) as the ratio of the reflected (transmitted) SPP power "just after" the mirror to

the incident power "just before" the mirror. In this way, the SPP-mirror reflectivity, R, could be determined from the PSTM images by computing the ratio:

$$R = \frac{I_M}{I_K}, \qquad (2)$$

where I_M and I_K denote, respectively, the SPP electric field intensity—magnitude detected by the PSTM—at observation points M and K located immediately after and immediately before the mirror [see Fig. 3(b)]. Nevertheless, because of the radiative scattering of the SPP produced by the mirror, this basic definition cannot be directly applied to obtain a reliable value of R. In fact, despite the metal layer coating the probes used in this work, the radiative contribution is too strong in this area and the PSTM signal recorded at these points is no longer proportional to the evanescent field intensity of either the incident or the reflected SPP, prohibiting the use of Eq. (2) for the calculation of R. In order to overcome this difficulty, the points used to determine R must be taken at a large enough distance from the mirror to prevent a significant contribution of the scattered light to the PSTM signal. However, when considering such observation points, M' and K', Eq. (2) has to be adapted to account for the intrinsic damping with propagation distance of the surface plasmon. The reflectivity can be then expressed as:
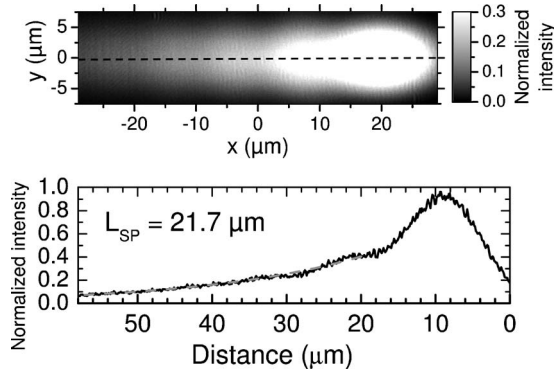
FIG. 4. (Upper image) PSTM image of a surface plasmon polariton (SPP) of wavelength corresponding to $\lambda_0 = 800$ nm propagating from right to left along a 50 nm thick gold metal film, without interaction with any defect. (Bottom graph) Intensity profile along the cross-cut marked by the dashed line in the PSTM image. By fitting the exponential decay of this intensity profile, the propagation length of the SPP can be determined.

$$R = \frac{I_{M'}}{I_{K'}} e^{(d_{M'} + d_{K'})/L_{SP}}, \qquad (3)$$

where $d_{M'}$ and $d_{K'}$ denote the distance between the points MM' and KK', respectively [see Fig. 3(b)] and L_{SP} represents the SPP propagation length (also called damping distance).

The computation of the reflectivity by means of Eq. (3) requires one to know the propagation length of the surface plasmon. Since L_{SP} depends strongly on the metal film thickness, its quality and its actual dielectric constant, we have determined it experimentally for each characterized SPP-Bragg mirror. Figure 4 shows the image of a surface plasmon polariton launched very close to the mirror to which corresponds Fig. 3(a), but without impinging on it. The electric field intensity evolution of this SPP is characterized, as expected, by an exponential attenuation with propagation distance due to the metal absorption.[2] The bottom graph in Fig. 4 shows the intensity profile taken along the dashed line drawn in the PSTM image. The SPP propagation length is obtained by fitting the intensity exponential decay to the following formula:

$$I = I_0 e^{-x/L_{SP}}. \qquad (4)$$

For the exponential fit, the first part of the profile, where the influence of the incident beam that excites the SPP is present, has to be discarded, since Eq. (4) corresponds to the intensity evolution of a freely propagating SPP.[24] For the SPP shown in Fig. 4, we find a propagation length value of $L_{SP} = 21.7 \pm 0.3$ μm. This value is in good agreement with the expected value for a 50 nm thick gold film, $L_{SP} = 25$ μm, calculated by using the dielectric constant of gold from Ref. 33, the difference between both values probably related to the gold film roughness ($rms = 1$ nm) and the possible variations in dielectric constant between our evaporated gold films and the data collected by Palik.[33]

Once the SPP damping distance is known, Eq. (3) allows us to obtain the SPP-mirror reflectivity. The solid line shown in Fig. 3(c) corresponds to the field intensity profile taken along the dashed line marked in Fig. 3(a), which goes through the center of the SPP incident beam (section A-B in the PSTM image) and through the center of the reflected beam (section B-C in the image). From any couple of points M' from section B-C of the profile and K' from section A-B we can compute R, and the final reflectivity associated to the mirror is then the average of these values. For the mirror shown in Fig. 3(a), and by averaging up to 10^4 couples of points, we obtain a mirror reflectivity value of $R = 80\% \pm 14\%$ (the uncertainty includes the deviation in the measure of L_{SP}, the error in the determination of the distances $d_{M'}$ and $d_{K'}$ and the dispersion in the average). This high value of the mirror reflectivity shows that the gratings of metal ridges are indeed very well suited to be used as SPP-Bragg mirrors and thus to control the propagation direction of surface plasmons.

As has been previously discussed, in order to compute the SPP-mirror reflectivity the procedure avoids to use data of the profile section around point B, since the radiative contribution, coming from the SPP radiative scattering induced by the mirror, is rather strong in this area and prevents an accurate measurement of the SPP near-field intensity. In order to estimate the influence of eventual radiative contributions in the detected near-field intensity along the incident and reflected SPP beams, we have recorded approach curves vertically to some selected points within these beams. The signal level far from the surface can be considered as merely radiative, because the SPP field intensity is strongly attenuated. Since the penetration depth of the SPP in air is $L_z \approx 340$ nm at $\lambda_0 = 800$ nm, this situation is practically reached at $z_0 = 1.5$ μm. This far-field intensity level is then compared with the level at the distance $z_0 \approx 150$ nm, where the PSTM images are recorded. For the incident beam, at 10 μm to the left of the mirror the radiative contribution is of the order of 1%. On the other hand, for the reflected beam the radiative contribution amounts to 6% at 12 μm away from the mirror, but decreases to 1% at 27 μm. This justifies that, for computing the mirror reflectivity, we need to restrict ourselves to points K' and M' in the profile section away from point B, but once this is observed the radiative contribution can be safely discarded.

The mirror transmission coefficient is calculated in a similar way. The solid line in Fig. 3(d) corresponds to the field intensity profile taken along the axis A-B (center of the incident beam) and B-D (center of the transmitted beam), marked by a dotted line in Fig. 3(a). The dashed line of Fig. 3(d) represents the computed intensity for the incident SPP by considering only the intrinsic damping. The ratio between both profiles provides the mirror transmission coefficient [see Eq. (3)]. For the mirror shown in Fig. 3, $T = 16\% \pm 3\%$, rather low since most of the SPP has been reflected. The dotted lines in Figs. 3(c) and 3(d) show the intensity profile of the freely propagating SPP that has been used to determine L_{SP} in this case. This profile overlaps the incident SPP beam almost perfectly, supporting the validity of the procedure to determine R and T.

The results exposed above indicate that the performance of the gratings of gold ridges as SPP-Bragg mirrors is very good, since a grating comprised of only 10 elements already
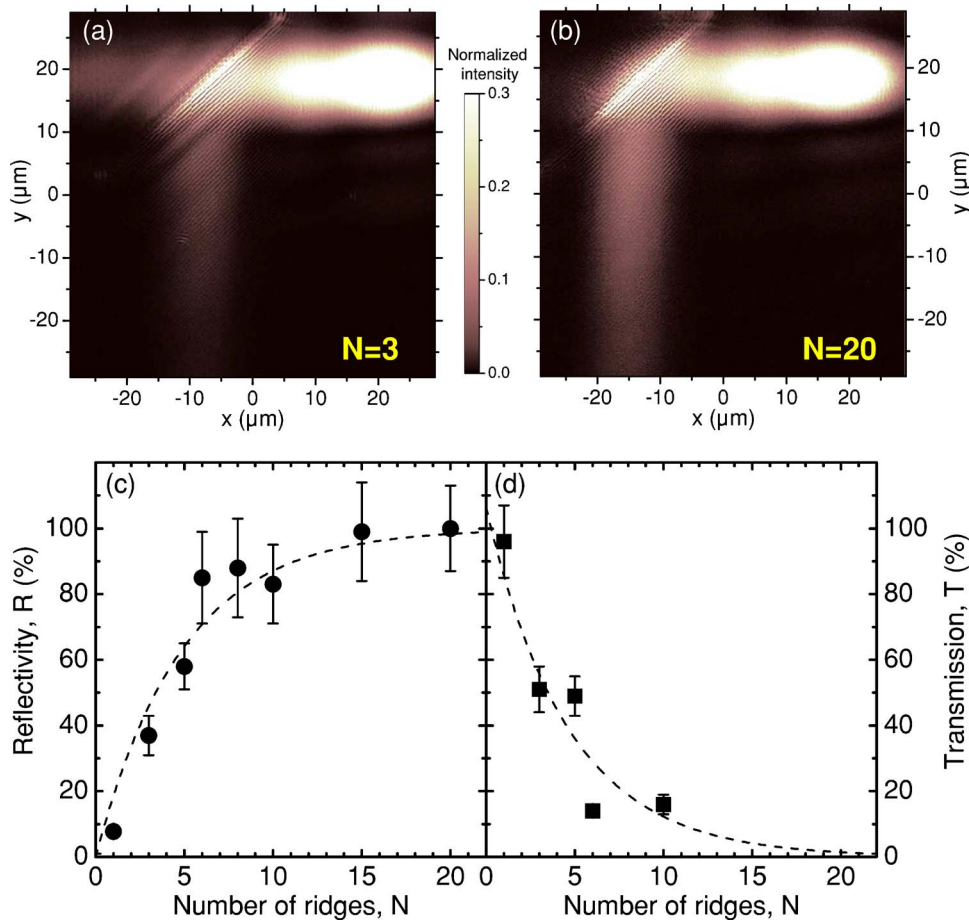
FIG. 5. (Color online) (a) Interaction of a surface plasmon polariton (SPP) with a SPP-Bragg mirror comprised of three gold ridges. The incoming plasmon travels from right to the left. (b) Same as (a), but for a mirror made of twenty gold ridges. (c) Evolution of the SPP-Bragg mirrors' reflectivity with the number of gold ridges composing the mirror. (d) Evolution of the SPP-Bragg mirrors' transmission coefficient with the number of mirror ridges. The dashed lines in (c) and (d) are guides to the eye.

provides a reflectivity of 80%. However, it would be interesting to know the evolution of the reflectivity with the number of ridges in the mirror, since this will determine the mirror size and hence constitutes a key issue for integration purposes. Figures 5(a) and 5(b) show the PSTM images of the interaction of SPP with two Bragg mirrors, consisting of 3 and 20 gold ridges, respectively. All other mirror characteristics are the same as those of the mirror shown in Fig. 3. The intensity of the incoming SPP is saturated to make the transmitted and reflected beams more visible. As can be seen from the images, the reflectivity of the mirror increases with the number of mirror elements and, accordingly, the transmission diminishes. Figures 5(c) and 5(d) show, respectively, the evolution of the Bragg mirrors' reflectivity and transmission coefficients as a function of the number N of gold ridges composing the mirror. The reflectivity increases very fast with the number of ridges, reaching a saturation value of $R=100\% \pm 15\%$ for $N=15$. The reflectivity values obtained for more than six gold lines are already higher than 50%, showing that very compact and efficient mirrors can be obtained with this arrangement. Consequently, the transmission coefficient decreases with the number of gold lines in the mirrors. In fact, from the PSTM images, the SPP transmission over $N=10$ is too weak to be determined over the radiative background.

These results indicate that the analyzed arrays of gold ridges are indeed very strong reflection gratings. Actually, even a single gold line provides a reflectivity of 8%. Besides,

while being within the mirror reflectivity gap, the losses produced by the system are low. The losses are obtained from the relationship $R+T+E=1$, where the SPP extinction E accounts for both scattering radiative losses and absorption within the mirror (the absorption in the metal during propagation is not considered due to the R and T determination procedure). From the data shown in Figs. 5(c) and 5(d), E is less than 10%.

Another interesting system to act as a SPP mirror consists of an array of slits engraved in the metal film. Figure 6(a) shows the PSTM image of a surface plasmon interacting with a SPP-Bragg mirror composed of ten grooves milled in the gold film. The width of the grooves is 200 nm, and they go through the full thickness of the gold layer. The period is again $d=557$ nm. As can be directly deduced from the image, the efficiency of this system is much lower than that of the gratings of gold lines. For the sake of an easy comparison, Fig. 6(b) presents the PSTM image of the reflection of a SPP by a mirror formed by 10 gold ridges. The reflectivity of the mirror made by slits, calculated from the near-field image, is $R=6\% \pm 3\%$, while for the equivalent system based on ridges we have measured values around 80%. This reduction in the mirror reflectivity does not imply a direct increase on the mirror transmission. In fact, the transmission coefficient of the grooves mirror has been estimated to be $T=16\% \pm 4\%$, a similar value to the one found for the equivalent lines mirror. From this result, we can conclude that the arrays of grooves introduce many more losses than the metal
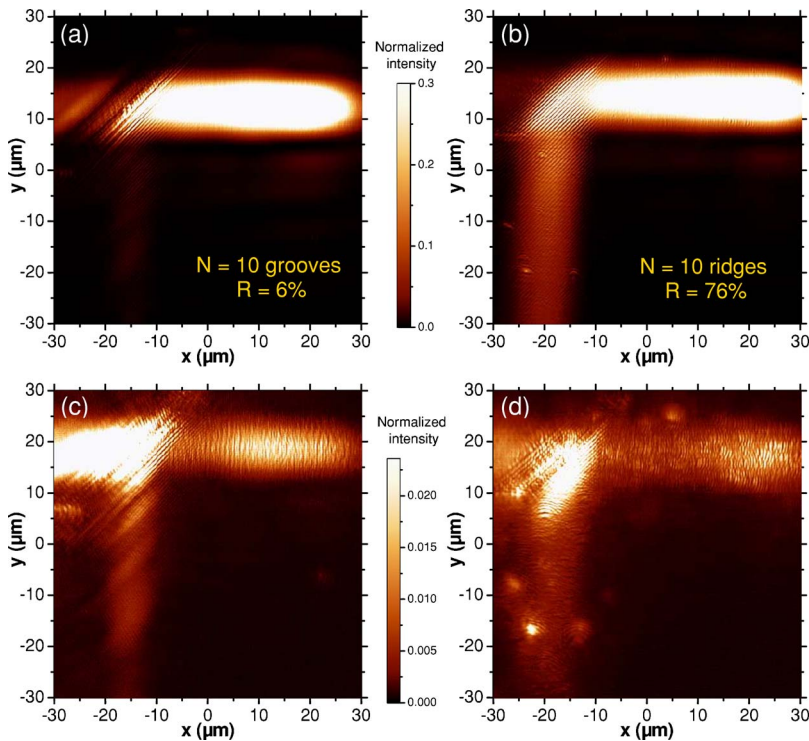
FIG. 6. (Color online) (a) PSTM image of the interaction of a surface plasmon (SPP) with a SPP-Bragg mirror consisting of 10 grooves engraved in a gold film. The reflectivity of the mirror is $R=6\% \pm 3\%$. (b) PSTM image of the interaction of a SPP with a mirror consisting of 10 gold lines. In this case, $R=76\% \pm 9\%$. (c) Same as (a), but taken 1.4 μm away from the surface. (d) Same as (b), but taken 1.4 μm away from the surface.

ridge gratings when interacting with the SPP: $E=78\% \pm 7\%$. These losses could be due to SPP scattering into radiative light, to coupling to a SPP propagating in the vertical walls of the grooves[6] or to coupling to SPP excited at the metal-glass substrate interface.[7] We cannot extract information on the two latter mechanisms from our near-field measurements, but we can still get some qualitative information on the radiative losses. As for the ridges mirrors, we have recorded approach curves vertically to some selected points within the incident, reflected and transmitted SPP beams in order to discriminate the radiative background from the evanescent field associated with the surface plasmon. The radiative contribution on the reflected beam amounts to 30% of the detected signal, which we interpret as a consequence of the very small near-field signal. In the transmitted beam, this radiative contribution represents 50% of the total signal, indicating the importance of radiative losses in this system. Moreover, the information extracted from the approach curves points out to stronger radiative losses in the forward direction, i.e., that of the transmitted beam, than in the backward or reflected direction.

To illustrate this last conclusion, Figs. 6(c) and 6(d) show, respectively, PSTM images of both kinds of Bragg mirrors, grooves- and ridges-based ones, at $z_0=1.4$ μm from the surface, where the SPP evanescent field intensity is negligible (2% of the value at $z_0=0$ μm since $L_z \approx 340$ nm) and the detected signal can be mainly associated with radiative components. In the first case, a neat radiative beam in the transmission direction appears, much stronger than the other contributions. For the lines grating, on the other hand, the distribution of the scattered intensities is weaker and much more homogeneous, with a bright spot located on the mirror itself. Besides, for Fig. 6(d), the scattering visible in the incoming and reflected beams for the mirror made of lines

seems to be originated by the metal film roughness, since its structure reproduces the surface defects. These radiative losses related to the metal film roughness are indeed taken into account in the determination of the propagation length of the surface plasmon, L_{SP} and, therefore, do not represent intrinsic losses of the SPP-Bragg mirror. Thus, the only radiative losses associated with the SPP mirror detected from this PSTM image is the bright area located on the mirror, and it should represent less than 10% of the total SPP power impinging in the mirror, as has been deduced above. On the other hand, in Fig. 6(c) the structure of scattering on the slits mirror transmitted and reflected beams looks much more like that of an outgoing radiated beam, thereby explaining the origin of the higher losses introduced by this kind of system. Nevertheless, it should be pointed out that the detection of these radiative losses does not preclude the presence of the other loss mechanisms mentioned above.

The higher efficiency of the arrays of ridges versus the arrays of slits for reflecting a surface plasmon is in good agreement with the behavior reported in Ref. 6. In this work, the interaction of a SPP with a step discontinuity is calculated for both going up and down steps, and the reflectivity is found to be much higher in the case of a raising step (ridge), the transmission through the step being similar in both cases. Moreover, this work also considers the radiated power in both cases, and the descending step results in a strong forward scattering, exactly as observed in the near-field characterization reported here.

An important aspect of the performance of Bragg mirrors is their spectral response. We have checked the spectral behavior of these SPP-Bragg mirrors within the tunability range of our laser (for $\lambda_0 \in [760, 820]$ nm), but no significant spectral differences have been found. This broad spectral response is indeed consistent with the fact that the mirrors'
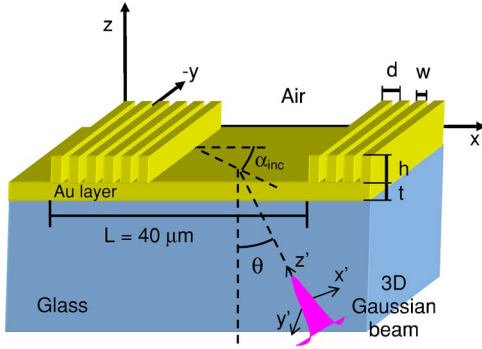
FIG. 7. (Color online) Sketch of the geometry considered for the numerical calculations: A three-dimensional gaussian beam impinging on a gold film (thickness t) deposited on glass at an angle θ excites a surface plasmon (SPP) in the gold film surface. This SPP travels on the gold-air interface and encounters, at an angle α_{inc}, an array of gold ridges (array periodicity d, ridges' width and height w and h, respectively). The system is infinite along the y axis and periodic, with period L, along the x axis.

reflectivity saturates for a low number of periods, since the mirror wavelength selectivity cannot be improved by the addition of more elements to the mirror grating. This kind of spectral behavior in SPP-Bragg mirrors has been already studied in detail in Ref. 12 for mirrors consisting of arrays of grooves, designed for normal incidence and integrated in SPP waveguides. Taking into account that the evolution of the mirrors' performance with the number of grating elements behaves in a similar way for those integrated mirrors and the mirrors considered in this work, we expect a similar spectral response. We would like to mention that, although broad, the Bragg mirrors do present a spectral selectivity, since mirrors fabricated with periods very different from those given by Eq. (1) did not deflect the incoming surface plasmon.

B. Numerical modeling of SPP-Bragg mirrors

To extend our analysis of SPP-Bragg mirrors, numerical calculations featuring configurations very close to the experimental ones have been carried out. The calculations are based on the formalism known as the differential method,[25,26] which allows the description of periodical systems. A scheme of the simulated geometry is shown in Fig. 7. The system consists of a gold thin film (thickness $t=50$ nm) deposited on glass and structured in such a way that it contains a finite array of gold squared ridges or grooves on the surface. Gold is described by the dielectric constant tabulated in Ref. 33, taking into account both the real and imaginary parts so that SPP damping is included in the calculations. The system is infinite along the y axis and periodic along the x axis with periodicity L. The gold film is illuminated by a three-dimensional (3D) focused Gaussian beam incoming from the glass substrate at the appropriate angle θ allowing to excite a SPP on the air-gold interface. The angle of incidence of the SPP on the Bragg mirror, α_{inc}, can be chosen by varying the in-plane orientation of the incoming Gaussian beam.

The description of a one-dimensional grating by means of the differential method relies on a truncated 1D planewave expansion of the electromagnetic field. For the conical incidence situation considered here, this expansion reads:

$$\mathbf{A}(x,y,z) = \sum_{m=-N}^{+N} \mathbf{A}(m)\exp[i(\alpha_m x + \beta_{inc}y + \gamma_m z)], \quad (5)$$

where $\mathbf{A}$ denotes the electric or magnetic field. The wave vector components of the planewaves are given by:

$$\alpha_m = n_1 k_0 \sin\theta\cos\alpha_{inc} + m\frac{2\pi}{L}$$

$$\beta_{inc} = n_1 k_0 \sin\theta\sin\alpha_{inc}$$

$$(\gamma_m^{1,2})^2 = (n_{1,2}k_0)^2 - \alpha_m^2 - \beta_{inc}^2, \quad (6)$$

$n_{1,2}$ being the refractive index of the substrate (glass) or the air, respectively. From Eq. (6) it is clear that the z wave vector component can be real or pure imaginary, introducing both radiative and evanescent orders in expansion (5). In our system, we have chosen a periodicity $L=40$ μm for $\alpha_{inc}=45°$ to prevent the interaction between contiguous mirrors, while keeping a reasonable computation time. The vertical discretization of the metal film and the number of harmonics in expansion (5) have been increased until a variation smaller that 1% has been achieved for SPP mirrors' computed reflectivity. Moreover, since the basic implementation of the differential method gives rise to numerical instabilities when introducing metallic objects, we have included the S-matrix propagation algorithm which solves this problem,[26–29] as well as an acceleration procedure denoted as "fast Fourier factorization (FFF)" method to improve the convergence of the field expansion (5) in the case of TM polarization.[26,30,31] To maintain the FFF method at a reasonable level of complexity,[32] the ridges or grooves composing the SPP-Bragg mirrors in the numerical simulations present completely vertical sidewalls.

As has been mentioned above, the gold film is illuminated by a 3D focused Gaussian beam, to reproduce the configuration used in the experimental characterization of the SPP-Bragg mirrors. To describe the Gaussian beam, the associated electric field is expanded as a 2D spectrum of planewaves in a local Cartesian coordinates system (x',y',z') taken in such a way that the z' direction is parallel to the propagation direction of the incident beam (see Fig. 7):[34]

$$\mathbf{E}'_{inc}(x',y',z')$$

$$= \int_{-\infty}^{+\infty} d\alpha' \int_{-\infty}^{+\infty} d\beta' \, \boldsymbol{\xi}'_{inc}(\alpha',\beta')$$

$$\times\exp[i\alpha'(x'-x'_f) + i\beta'(y'-y'_f) + i\gamma(\alpha',\beta')(z'-z'_f)]. \quad (7)$$

In this expression, (x'_f, y'_f, z'_f) denotes the position of the Gaussian beam focal point in the local coordinates system; the z' component of the each harmonic wave vector is given by: $\gamma(\alpha',\beta')=(n_1^2 k_0^2 - \alpha'^2 - \beta'^2)^{1/2}$; and the Gaussian shape
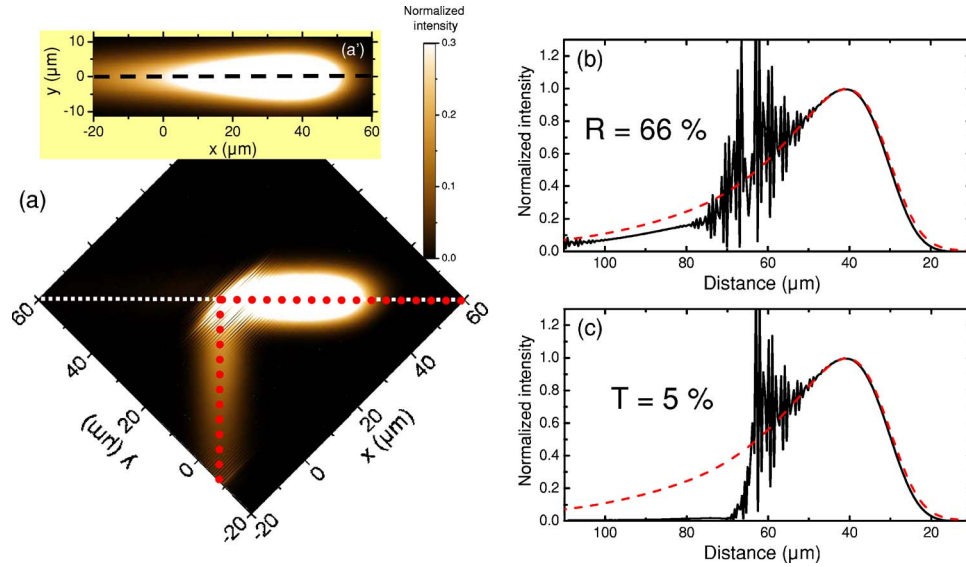
FIG. 8. (a) (Color online) Calculated electric field intensity map at z_0=150 nm from the gold surface for the interaction of a surface plasmon polariton (SPP) propagating on a gold surface with an array of gold ridges, or SPP-Bragg mirror. The array consists of 11 gold lines, 50 nm high and 150 nm wide, with a periodicity of d=557 nm, and the incoming SPP (λ_0=800 nm) arrives at α_{inc}=45°. The position of the array in the image is marked by the deflection of the SPP. (a′) For the sake of reference, calculated electric field intensity map for a surface plasmon propagating freely on a non-structured 50 nm thick gold film. (b) (Solid line) Profile of the field intensity taken along the red big dotted line drawn in (a). From this profile, the obtained mirror reflectivity is R=66% ±2%. (Dashed line) Profile of the field intensity along the dashed line plotted in (a′). (c) (Solid line) Profile of the field intensity through the white small dotted line drawn in (a). (Dashed line) Same as in (b). The obtained mirror transmission coefficient in this case is T=5% ±1%.

of the beam is determined by the Fourier amplitudes:

$$\xi'_{inc}(\alpha',\beta') = \mathbf{e}'(\alpha',\beta')\exp[-w_0(\alpha'^2 + \beta'^2)/4]. \quad (8)$$

The beam waist w_0 controls the lateral size of the beam in the focal plane, and the TM polarization of the beam is introduced by:

$$e'_{x'}(\alpha',\beta') = 1, \quad e'_{y'}(\alpha',\beta') = 0, \quad \forall\, \alpha',\beta'.$$

The planewave expansion of the Gaussian beam is truncated such that the harmonics traveling towards the negative values of z are excluded.[34] Once the Fourier spectrum on the Gaussian beam is defined in the local coordinates system, each harmonic is rotated to the global coordinates system (x,y,z)[34] and the differential method is applied for each harmonic. Note that, except for the fundamental harmonic (0,0), each harmonic of the Gaussian beam corresponds to a set of two angles θ and α_{inc} that is different from that of the beam itself. Finally, the electric field intensity map in the plane $z=z_0$ over the gold film is recovered from the sum of the field amplitudes of all the beam harmonics. This electric field intensity map is then directly compared with the experimental PSTM images of the SPP-Bragg mirrors, since it has been shown that for this kind of collecting probe near-field microscopy the recorded images are in good agreement with the electric near fields computed without including any tip.[35]

Figure 8(a) shows the calculated electric field intensity map at z_0=150 nm, corresponding to the interaction of a SPP with a SPP-Bragg mirror consisting of 11 gold ridges, 50 nm high and 150 nm wide and periodicity d=557 nm, adequate for an incident Gaussian beam of wavelength λ_0=800 nm

arriving at α_{inc}=45°, as in the experimental configuration. The Gaussian beam is focused at 25 μm from the mirror first line. The similarity between the obtained map and the experimental PSTM images is remarkable. The SPP is strongly deflected by the SPP mirror, as in the experimental case, and only a small portion of it is transmitted through the mirror. The mirror reflectivity and transmission coefficients have been determined by using the same procedure as in the analysis of the experimental data. The electric field intensity map of a SPP propagating freely on a nonstructured metal surface is also shown in Fig. 8(a′). From this image, L_{SP}=25 μm is extracted. Figures 8(b) and 8(c) show the intensity profiles through the reflected and transmitted beams on the calculated map (solid lines) together with the profile along the freely propagating SPP (dashed lines). From these profiles and applying Eq. (3), we obtain the reflectivity and transmission coefficients of the simulated SPP-Bragg mirror: R=66% ±2% and T=5% ±1% in this case. The agreement with the experimental result is good, although the reflectivity value extracted from the numerical simulation is lower than the experimental value. We associate this discrepancy with the differences in shape between the experimental and the simulated ridges. In the former case, the edges of the ridges are softer than in the last one, where due to computing time constraints the defined ridges' edges are perfectly sharp. Sharp edges are likely to provide a higher scattering than soft ones, therefore accounting for the reduced reflectivity obtained for the simulated mirrors.

Figure 9 shows the evolution of the reflectivity, transmission coefficients, and losses for the simulated Bragg mirrors as a function of the number of ridges composing the mirror. The obtained results are in perfect consistency with the ex-
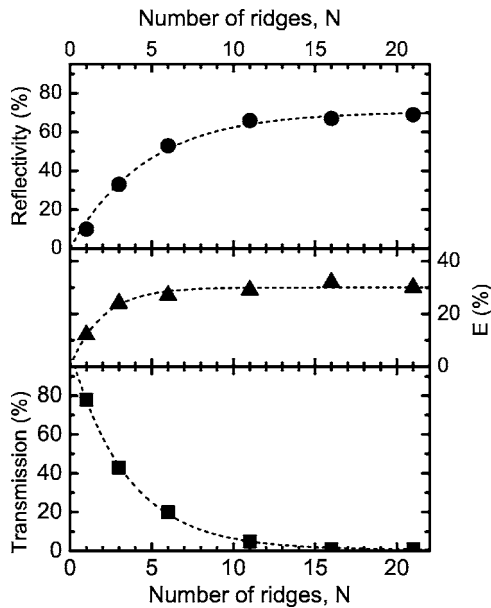
FIG. 9. (Upper graph) Evolution of the SPP-Bragg mirrors' reflectivity with the number N of gold ridges of the grating, obtained from the numerical calculations. (Middle graph) Evolution of the system losses with N. (Bottom graph) Evolution of the mirror's transmission coefficient with N.

perimental data. The reflectivity saturates for a reduced number of gold ridges, $N \approx 10$, and the increasing rate of reflectivity is very close to that obtained experimentally for the equivalent kind of mirrors. The transmission coefficient decreases with N, as can be expected, and the losses become higher due to the increasing number of scattering elements. The saturation of the mirror reflectivity for a given value N of ridges implies that the SPP interacts with this given number of mirror elements. The addition of more ridges does not affect the system since they are not attained. Consequently, losses should not increase either for higher values of N, which is indeed observed from the exposed results. The reflectivity obtained from a simulated mirror made of only one gold line is $R = 10\%$, a little bit higher than that measured experimentally, $R = 8\%$. Evidently, this could be due to the existing differences between the experimental and the simulated geometry (ridges' height and width), but it is also possible that it is a consequence of the edge profile. A sharp edge, as in the simulated case, is likely to provide a stronger reflectivity than a softer one. However, since the scattering is also increased, the transmission would decrease, as it actually does ($T = 78\%$ for the simulated case versus $T > 90\%$ for the experimental one). Hence, this reduction in the transmission for the calculated mirrors explains that experimental and calculated data show a small misfit in the number of mirror elements for which the reflectivity saturates.

Figures 10(a) and 10(b) show the calculated electric field intensity maps for two mirrors made of 11 grooves and lines, respectively. Both the lines' and the grooves' width is 150 nm, the lines' height is 50 nm and the grooves depth too. As for the experimental situation, the images show undoubtedly that the ridges-based system is a more efficient SPP mirror than the array of slits. The reflectivity value obtained
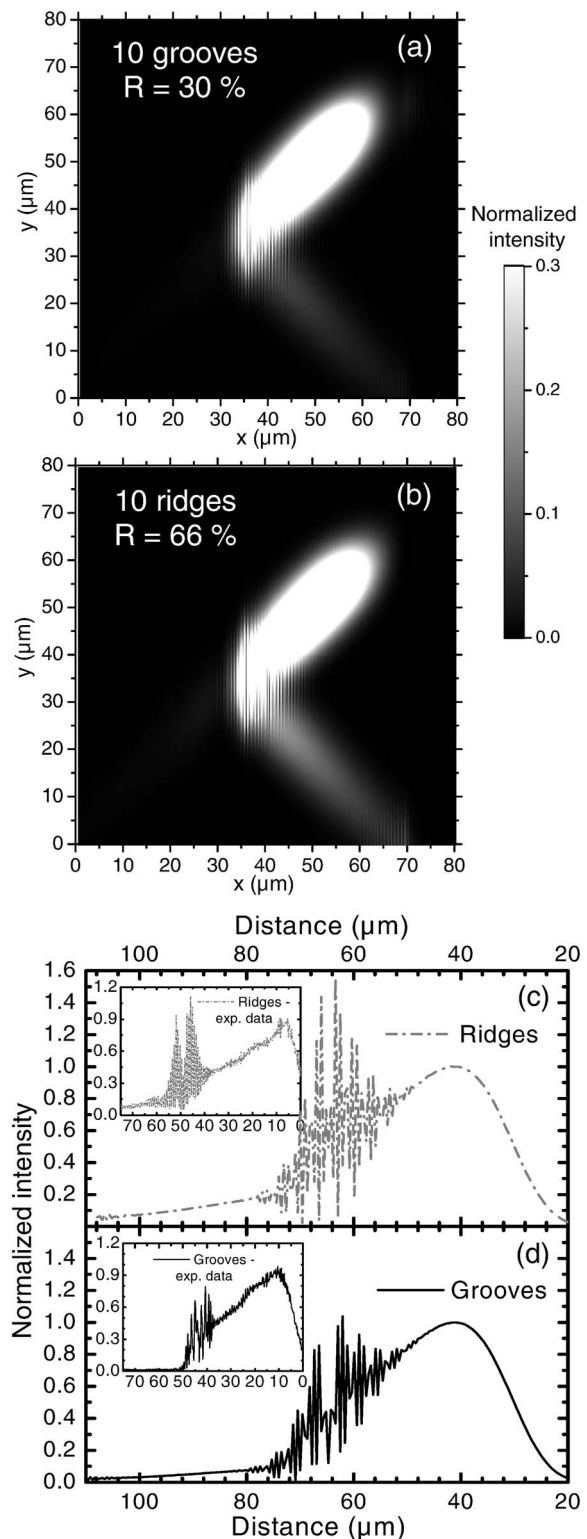

FIG. 10. (a) Calculated electric field intensity map of a surface plasmon interacting with a SPP-Bragg mirror made of 11 grooves. The mirror reflectivity is $R = 30\%$. (b) Same as (a), but for a mirror composed of 11 gold lines ($R = 66\%$). (c) Intensity profile taken along the incident and reflected SPP beams for the mirror made of ridges. The inset in the graph corresponds to the same profile, but taken from the experimental PSTM image shown on Fig. 6(b). (d) Same as (c), but for the grooves-based mirror. The inset corresponds to a profile taken from the PSTM image shown in Fig. 6(a).

for the grating of grooves is $R=30\% \pm 1\%$, and the transmission coefficient $T=2\%$, which implies that this system gives rise to a high amount of losses, as had already been concluded in the precedent section. In this case, the experimental value of reflectivity is smaller than the calculated one. We attribute this difference again to the actual differences between the simulated and experimental edge profiles: The simulated edges are sharp, but the fabricated slits have rough edges, as can be seen in the zoom of Fig. 1(d), and their reflecting power is lower since they introduce more diffuse scattering losses, not necessarily radiative.

The good agreement found between the results obtained from the simulations and the experimental data proves the reliability of the employed calculation procedure. Numerical calculations can then be used to test different configurations at the design stage. An absolute quantitative agreement between theory and experiment has not been achieved, but this can be understood because of the unavoidable differences between the simulated defect profiles and the fabricated ones. Furthermore, not only overall tendencies on the SPP interaction with surface defects are well reproduced by the calculations, but also some details. So, Figs. 10(c) and 10(d) show the calculated intensity profiles taken along the incident and reflected SPP beams for SPP-Bragg mirrors made of ridges and grooves, respectively. Even though the grooves mirror introduces higher losses than the lines one, the intensity spikes present over the mirror (central part of the profiles) are lower. The same behavior has been indeed obtained from the experimental near-field images (the experimental profiles are shown in the insets of the graphs).

IV. DISCUSSION

The experimental data presented in Sec. III A show that the arrays of gold lines act as efficient mirrors, providing a high reflectivity for a relatively low number of mirror elements. This result implies that a metal ridge is in fact a strongly reflecting system for SPP propagating on extended thin films. Consequently, and although the reflectivity achieved for a mirror composed by a small number of ridges will be strong, the spectral selectivity of the mirror will be rather limited. The increase on the number of mirror elements will not provide a thinner spectral response, since the interaction is restricted to a small number (around 15) of metal lines, for which the mirror reflectivity reaches its saturation value. Moreover, the strong reflecting power of the arrays of metal ridges is not due the alternation of media with different effective index of refraction, n_{eff}, for the SPP, as it is the case in the classical Bragg mirrors consisting of periodical stacks of dielectric layers, or as has been recently suggested for SPP based on metal heterostructures.[36] To allow a strong reflection for a small number of interfaces, the variation of n_{eff} has to be considerable, with the consequent change of SPP wave vector modulus within the different media, and the periodicity of the adequate grating will not obey the simple geometrical diffraction relation given by Eq. (1). This equation should indeed be corrected by the appropriate n_{eff} for each media constituting the mirror. Conversely, the SPP-Bragg mirrors composed of metal ridges are based on
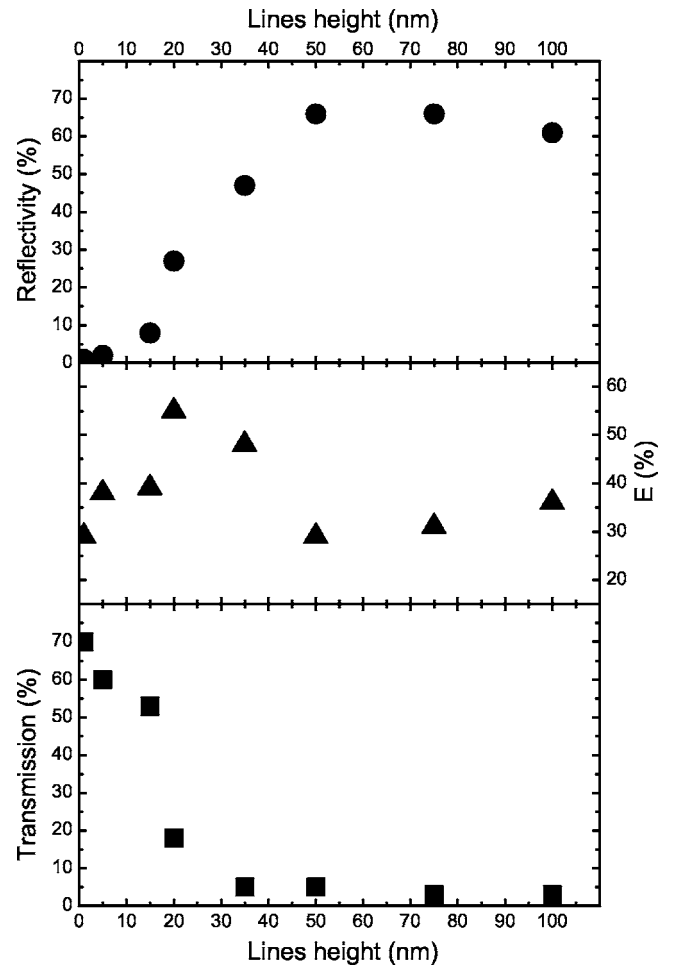

FIG. 11. Evolution of the reflectivity (circles), transmission coefficient (squares), and losses (triangles) for SPP-Bragg mirrors consisting of arrays of 10 gold ridges as a function of the ridge height. The gold lines' width is 150 nm in all cases.

the existence of a photonic bandgap on a periodically corrugated surface,[37,38] where the gap position in wave vector is evidently determined by the system periodicity and corresponds to the boundary of the first Brillouin zone, which is equivalent to Eq. (1). The experimental data shown in this work demonstrate that the presence of this photonic bandgap gives rise to an efficient SPP reflection for conical propagation at 45°.

It is expected that the gap width, and hence the reflectivity power of the mirrors, increases with the modulation height.[38] By using our numerical simulations, which were proven in Sec. III B to correctly describe the behavior of the metal lines gratings, we have analyzed the evolution of the 45° mirrors' reflectivity as a function of the lines' height. Figure 11 shows the obtained values for the reflectivity (circles), transmission coefficient (squares), and losses (triangles) for mirrors made of lines of several heights. All the gratings consist of eleven gold lines, and the width is 150 nm. As expected, the reflectivity rises with the ridges' height, but it reaches a saturation value for lines of around 50 nm; the transmission exponentially decreases as the ridges become higher. The behavior of the system losses is more complex.

For very small heights, the perturbation introduced by the corrugation does not deflect efficiently the incoming SPP. Nevertheless, it affects the SPP mode passing through, deforms it and gives rise to losses, probably radiative scattering. A little increase in the defects' height produces a better reflection but it mainly augments the losses, since the deformation induced in the mode becomes bigger being larger the interaction area. A further increase in height, however, makes the ridges array to reflect very efficiently the incident SPP and the losses are drastically reduced. This behavior suggests that the interaction of the SPP with the surface defects is mostly located in a zone very close to the surface, which seems reasonable due to the exponentially decaying character of the SPP field. When in this "very-close-to-the-surface" zone the SPP finds an edge, the interaction results mainly in radiative scattering and the losses are large. On the other hand, if it is a barrier that the surface plasmon experiences there, it will be efficiently reflected. From the simulations, the "very-close-to-the-surface" zone represents a height of around 50 nm. Moreover, if the ridges' height becomes too big ($h \geq 100$ nm), losses increase again and the mirror efficiency goes down.

V. CONCLUSIONS

Summarizing, this work demonstrates that an array of metal ridges can very efficiently deflect a surface plasmon polariton propagating on a metal surface. By means of near-field optical microscopy, we have characterized the performance of these SPP-Bragg mirrors working at 45° incidence and, from these measurements, quantitative information on their reflectivity and transmission power has been obtained. A mirror made of 15 gold lines has been shown to reflect almost the total incident SPP. Arrays of slits engraved in the metal have also been analyzed, and their reflectivity proved to be much smaller than that of the gratings of metal lines. This has been attributed to the stronger forward scattering produced by the grooves. Finally, numerical calculations based on the differential method have been carried out for this kind of SPP-Bragg mirrors. The obtained results show an excellent agreement with the experimental data, reproducing all the tendencies found in the experimental study. This confirms the reliability of the numerical procedure employed as a predicting and modeling tool of SPP optical elements.

*Electronic address: Maria-Ujue.Gonzalez@u-bourgogne.fr

[1] W. L. Barnes, A. Dereux, and T. W. Ebbesen, Nature (London) **424**, 824 (2003).

[2] H. Raether, *Surface Plasmons on Smooth and Rough Surfaces and on Gratings*, Vol. 111 of Springer Tracts in Modern Physics (Springer-Verlag, Berlin, 1988).

[3] S. I. Bozhevolnyi and F. A. Pudonin, Phys. Rev. Lett. **78**, 2823 (1997).

[4] J. A. Sánchez-Gil and A. A. Maradudin, Phys. Rev. B **60**, 8359 (1999).

[5] A. V. Shchegrov, I. V. Novikov, and A. A. Maradudin, Phys. Rev. Lett. **78**, 4269 (1997).

[6] H. A. Jamid and S. J. Al-Bader, IEEE Photonics Technol. Lett. **9**, 220 (1997).

[7] J. Seidel, F. I. Baida, L. Bischoff, B. Guizal, S. Grafström, D. VanLabeke, and L. M. Eng, Phys. Rev. B **69**, 121405(R) (2004).

[8] I. I. Smolyaninov, D. L. Mazzoni, and C. C. Davis, Phys. Rev. Lett. **77**, 3877 (1996).

[9] J. C. Weeber, Y. Lacroute, and A. Dereux, Phys. Rev. B **68**, 115401 (2003).

[10] R. Charbonneau, P. Berini, E. Berolo, and E. Lisicka-Shrzek, Opt. Lett. **25**, 844 (2000).

[11] A. Drezet, A. L. Stepanov, H. Ditlbacher, A. Hohenau, B. Steinberger, F. R. Aussenegg, A. Leitner, and J. R. Krenn, Appl. Phys. Lett. **86**, 74104 (2005).

[12] J.-C. Weeber, Y. Lacroute, A. Dereux, E. Devaux, T. Ebbesen, C. Girard, M. U. González, and A.-L. Baudrion, Phys. Rev. B **70**, 235406 (2004).

[13] H. Ditlbacher, J. R. Krenn, G. Schider, A. Leitner, and F. R. Aussenegg, Appl. Phys. Lett. **81**, 1762 (2002).

[14] A. Hohenau, J. R. Krenn, A. L. Stepanov, A. Drezet, H. Ditlbacher, B. Steinberger, A. Leitner, and F. R. Aussenegg, Opt. Lett. **30**, 893 (2005).

[15] W. L. Barnes, S. C. Kitson, T. W. Preist, and J. R. Sambles, J. Opt. Soc. Am. A **14**, 1654 (1997).

[16] S. I. Bozhevolnyi, J. Erland, K. Leosson, P. M. W. Skovgaard, and J. M. Hvam, Phys. Rev. Lett. **86**, 3008 (2001).

[17] D. Egorov, B. S. Dennis, G. Blumberg, and M. I. Haftel, Phys. Rev. B **70**, 033404 (2004).

[18] E. Devaux, T. W. Ebbesen, J.-C. Weeber, and A. Dereux, Appl. Phys. Lett. **83**, 4936 (2003).

[19] J. A. Sánchez-Gil and A. A. Maradudin, Appl. Phys. Lett. **86**, 251106 (2005).

[20] S. I. Bozhevolnyi, A. Boltasseva, T. Søndergaard, T. Nikolajsen, and K. Leosson, Opt. Commun. **250**, 328 (2005).

[21] S. Jetté-Charbonneau, R. Charbonneau, N. Lahoud, G. Mattiussi, and P. Berini, Opt. Express **13**, 4674 (2005).

[22] V. Coello, T. Søndergaard, and S. I. Bozhevolnyi, Opt. Commun. **240**, 345 (2004).

[23] R. C. Reddick, R. J. Warmack, and T. L. Ferrell, Phys. Rev. B **39**, 767 (1989).

[24] P. Dawson, F. de Fornel, and J.-P. Goudonnet, Phys. Rev. Lett. **72**, 2927 (1994).

[25] P. Vincent, Opt. Commun. **26**, 293 (1978).

[26] M. Nevière and E. Popov, *Light Propagation in Periodic Media: Differential Theory and Design* (Marcel Dekker, New York,

2003).

[27] F. Montiel and M. Nevire, J. Opt. Soc. Am. A **11**, 3241 (1994).

[28] L. Li, J. Opt. Soc. Am. A **11**, 2829 (1994).

[29] L. Li, J. Opt. Soc. Am. A **13**, 1024 (1996).

[30] L. Li, J. Opt. Soc. Am. A **13**, 1870 (1996).

[31] L. Li, J. Opt. Soc. Am. A **14**, 2758 (1997).

[32] E. Popov and M. Nevire, J. Opt. Soc. Am. A **18**, 2886 (2001).

[33] *Handbook of Optical Constants of Solids*, edited by E. D. Palik (Academic, San Diego, 1985).

[34] J. C. Weeber, A. Dereux, C. Girard, G. Colas des Francs, J. R. Krenn, and J. P. Goudonnet, Phys. Rev. E **62**, 7381 (2000).

[35] A. Dereux, E. Devaux, J. C. Weeber, J. P. Goudonnet, and C. Girard, J. Microsc. **202**, 320 (2001).

[36] B. Wang and G. P. Wang, Appl. Phys. Lett. **87**, 013107 (2005).

[37] M. Kretschmann, T. Leskova, and A. Maradudin, Opt. Commun. **215**, 205 (2003).

[38] W. L. Barnes, T. W. Preist, S. C. Kitson, and J. R. Sambles, Phys. Rev. B **54**, 6227 (1996).